






Interplay of field-induced molecular dipole alignment and compensating surface polarization in low-temperature P - V hysteresis of $\text{MAPbBr}_3(001)$

Lars Freter ¹, Hung-Chang Hsu,² Raman Sankar,^{3,4} Chun-Wei Chen,^{4,5} Rafal E. Dunin-Borkowski ¹, Philipp Ebert ¹,
Ya-Ping Chiu ^{2,3,*} and Michael Schnedler ^{1,†}

¹Ernst Ruska-Centrum (ER-C 1) and Peter Grünberg Institut (PGI 5), Forschungszentrum Jülich GmbH, 52425 Jülich, Germany

²Department of Physics, National Taiwan University, 10617 Taipei, Taiwan

³Institute of Physics, Academia Sinica, 11529 Taipei, Taiwan

⁴Center for Condensed Matter Sciences, National Taiwan University, 10617 Taipei, Taiwan

⁵Department of Materials Science and Engineering, National Taiwan University, 10617 Taipei, Taiwan

 (Received 18 October 2022; revised 9 February 2023; accepted 19 April 2023; published 10 May 2023)

We demonstrate the presence of a hysteresis in tunneling spectra acquired at 4.3 K on cleaved MA-Br terminated (001) surfaces of MAPbBr_3 single crystals. Simulations of the tunneling spectra reveal an underlying polarization-voltage (P - V) hysteresis, which is caused by an interplay of subsurface field-induced rotation and alignment of the MA molecules, stabilized by dipole-dipole interactions, and an ion-lattice relaxation. The resulting subsurface polarization is counteracted by a compensating surface polarization, detectable by surface-sensitive tunneling spectroscopy.

DOI: [10.1103/PhysRevMaterials.7.L052401](https://doi.org/10.1103/PhysRevMaterials.7.L052401)

Metalorganic halide perovskites attracted extraordinary attention as low-cost photovoltaic absorber materials, exhibiting an unexpectedly rapid increase of the conversion efficiency within a few years only [1–3]. However, it is unclear to what degree the reported conversion efficiencies extracted from current density versus voltage (J - V) curves are accurate, since J - V hystereses are known to make “bad cells look good” [4]. It is thus of paramount importance to unravel the physical mechanisms inducing J - V hysteresis, but no consent has been achieved yet. Instead, the proposed physical mechanisms widely range [5–7] from ferroelectricity [8–13], to ion migration [14–18] to charge trapping-detrapping [19], believed to compete with and mutually exclude each other [15]. The lack of clarity is likely aggravated on the one hand by significant differences in the materials’ quality. On the other hand, probing and quantifying directly local polarizations, notably at surfaces/interfaces, is a very delicate task. In addition, J - V measurements are usually only performed at room temperature, i.e., under an operating condition of solar cells, limiting the access to the underlying physical mechanisms. Low temperatures would allow a discrimination of the different physical effects by freezing out ion migration/drift as well as charge trapping-detrapping-induced hystereses.

Here, we demonstrate the presence of a ferroelectric hysteresis in scanning tunneling spectra on high-quality single-crystal methyammonium lead bromide (MAPbBr_3)(001) even at 4.3 K. By quantifying the polarization versus applied voltage, we unravel a delicate interplay of subsurface field-induced rotation and alignment of the methyammonium (MA) molecules, stabilized by dipole-dipole interactions, and

co-occurring ion-lattice relaxation, both counteracted by a compensating surface polarization. The results suggest that the dominating physical effect at the origin of hysteresis changes with temperature.

As a model system we investigate MA-Br terminated (001) surfaces of MAPbBr_3 single crystals cleaved in ultrahigh vacuum at 4.3 K using scanning tunneling microscopy (STM) and spectroscopy (STS). We chose this surface termination, since it contains MA molecules directly in the surface layer [cf. the conceptual drawing of the cleavage surface in Fig. 1(a)]. In contrast, the Pb-Br terminated cleavage surface does not contain MA molecules and is also less stable [20]. At the chosen measurement temperature of 4.3 K, MAPbBr_3 is in its orthorhombic phase and constant-current STM images reveal extended atomically flat terraces, exhibiting an ordered dimer structure along the [110] direction [Fig. 1(b)] [21]. The measured lattice constants of 0.78 and 0.82 nm corroborate that the investigated surface is $\text{MAPbBr}_3(001)$. The bright protrusions imaged are revealing the negatively charged Br^- positions, since at large negative sample voltage electrons tunnel out of the filled states of the Br^- surface anions. In contrast, the MA^+ molecules (cations) remain hidden, since their density of states extending into the vacuum is lower [22]. The Br dimer structure is related to the in-plane antiferroelectric ordering of the MA molecule dipoles [22–25]. This order is visualized by the white arrows in the inset of Fig. 1(b), revealing head-to-head (positive sides of molecule dipoles facing each other) and tail-to-tail configurations [22]. The dimer structure remains present at all acquisition voltages used [Fig. 1(c)].

Figure 2 illustrates a typical averaged I - V spectrum in logarithmic scale measured at 4.3 K. Blue circles correspond to the forward voltage sweep (i.e., from negative to positive voltages), while red symbols indicate the backward sweep.

*ypchiu@phys.ntu.edu.tw

†m.schnedler@fz-juelich.de

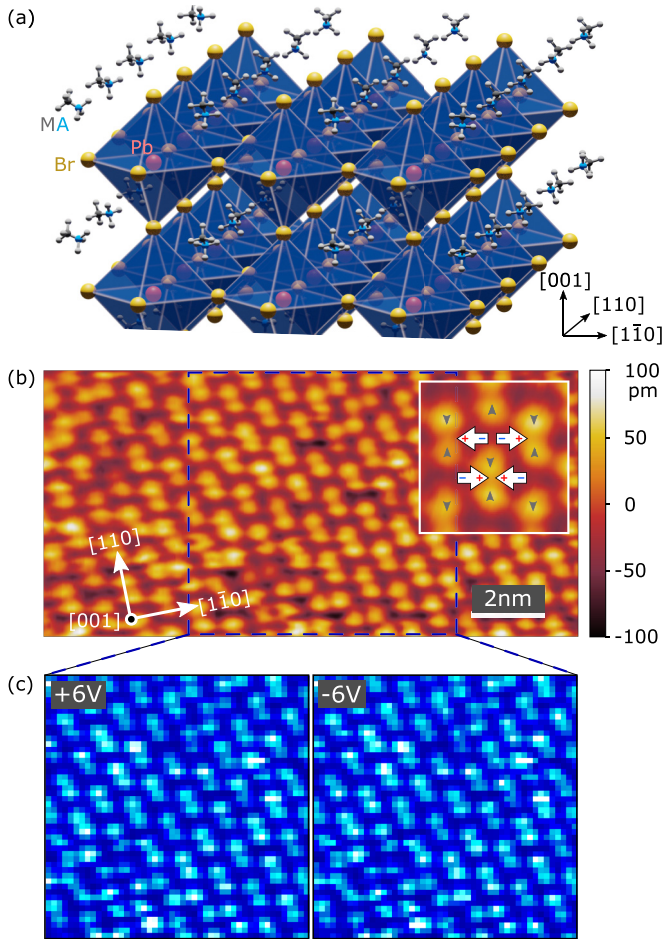


FIG. 1. (a) Conceptual schematic ball model of the MA-Br terminated (001) cleavage surface of a MAPbBr_3 crystal (simplified by using the cubic phase at room temperature). Below ~ 145 K tilting of the PbBr_6 octahedra reduces the symmetry leading to an orthorhombic phase, which was investigated experimentally at 4.3 K [12,31]. (b) Constant current STM image of the (001)-cleaved orthorhombic phase acquired at 4.3 K and a set point of -6 V and 0.2 nA. Bright protrusions correspond to the filled states at the Br^- surface ions. They form a dimer structure along the $\langle 110 \rangle$ direction due to the interplay of surface relaxation and MA dipole ordering. Inset: High-resolution STM image. White arrows indicate the dipole orientation of the intercalated MA molecules inducing a relaxation of the surrounding Br^- ions. (c) Normalized current imaging tunneling spectroscopy (CITS) maps, corrected for the spatial changes in tip-sample separation induced by the constant current feedback loop evaluated at $+6$ V (left map) and -6 V (right map).

A hysteresislike behavior can be recognized: Within the voltage range between -5 to $+6$ V the two I - V spectra differ significantly. Plateaus with almost constant tunnel current in the range of 0.1 nA are present at negative, i.e., -1 to -4 V, (positive, $+2$ to $+5$ V) voltages for the backward (forward) sweep direction, with steep current transitions in between. At the voltages of these plateaus, the opposite sweep direction exhibits no detectable tunnel current (below the noise level). For large absolute voltages, i.e., < -5 and $> +6$ V, the tunnel currents of the forward and backward spectrum coincide again. Note, the tunneling spectra measured on the dimer and

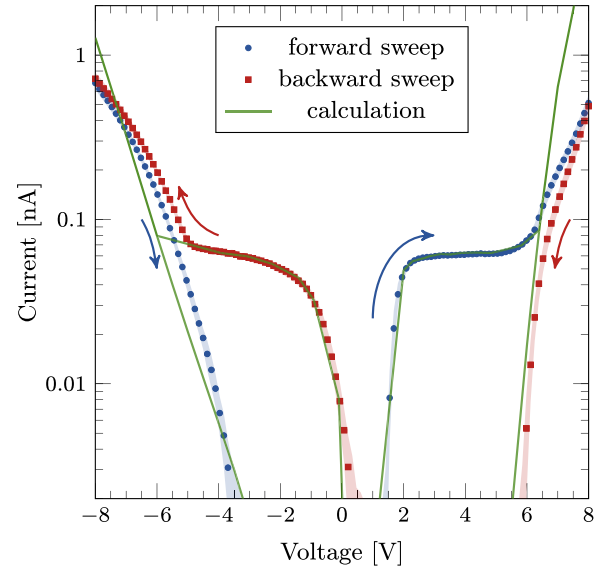


FIG. 2. Scanning tunneling spectroscopy of the cleaved MAPbBr_3 single-crystal (001) surface acquired at 4.3 K. The symbols represent the I - V spectrum averaged from about 5000 single spectra. The background shadow indicates the standard deviation of the average. The forward (backward) sweep is indicated by blue (red) symbols and by additional arrows. The slew rate of 33.5 V/s is identical for both voltage sweep directions. A set point of -6 V and 0.20 nA was used before interruption of the feedback loop. Theoretical computations of the tunnel current assuming a polarization change are shown as green lines (see text for details).

zigzag structures as well as at boundaries and defect sites reveal no differences within the measurement accuracy.

In order to quantitatively understand the hysteresis in the measured tunneling spectra, it is necessary to address the origins of the tunnel current and the prime factors influencing it. For semiconductors, the tunnel current at negative and positive voltages arises from electrons tunneling out of the valence and into the conduction band states, respectively. The onset voltages indicate the band-edge positions, which can be shifted to larger voltages due to the presence of a so-called tip-induced band bending, i.e., the penetration of the applied electric field into the semiconductor [26,27]. The degree of penetration is influenced by screening through free charge carriers and a potential presence of spontaneous as well as field-induced electric polarization. Hence, the tunnel current is sensitive to both the free charge carrier redistribution and the electric polarization at the surface. Note, the current transitions between the plateaus are not related to field emission resonances [28], since the transitions occur at effective energies smaller than the tip/sample work function due to the large tip-induced band bending and surface polarization modifying the band structure/alignment. Furthermore, no defects are generated.

The presence of hysteresis at 4.3 K thus suggests a delayed response of either the redistribution of free charge carriers or the change of electric polarization. Free charge carriers can be ruled out as the origin of the hysteresis, because their redistribution occurs in a femtosecond timescale [29], which is much shorter than the voltage sweep. Hence the electric polarization has to be addressed. Note, all other effects proposed so far as

the potential origin for the hysteresis such as ion migration and charge trapping-detrapping are frozen out at 4.3 K and cannot influence the tip-induced band bending [30].

Therefore, we focus on unraveling the bias-dependent changes of the polarization at the MAPbBr₃(001) surface. For this we employ theoretical tunnel current computations and compare the results to the experimental tunnel spectra (cf. green lines in Fig. 2 as an example) [32–34]. The MAPbBr₃ sample is modeled as an *n*-type semiconductor with a (low-temperature) relative permittivity of 26 [31,35], an electron affinity of 3.7 eV [36], and a band gap of 2.3 eV [37–40]. The polarization in the [001] direction, the free carrier concentration, as well as the tip-sample separation are fit parameters [41]. Standard values for all further parameters are used, since they only have a minor influence. The fit is executed in a two-step process: First, for each voltage sweep direction, the polarization and tip-sample separation are adjusted to obtain good agreement at all voltages outside the two plateaus. The there obtained saturation (or remanent) polarization values are $P_{\text{sat,max}} = -16 \mu\text{C}/\text{cm}^2$ and $P_{\text{sat,min}} = -6.4 \mu\text{C}/\text{cm}^2$ at tip-sample separations of 7.5 and 9.65 Å, respectively, assuming a free carrier concentration of $3.5 \times 10^{17} \text{ cm}^{-3}$. Second, the plateaus in the measured *I-V* spectra are simulated as transition regions, where the polarization and tip-sample separation change gradually with voltage between the above determined limits. For this purpose a linear approximation of the tip-sample separation on the polarization is used, as discussed later. This procedure is repeated for a range of different bulk charge carrier concentrations (i.e., $3.5 \times 10^{17} \text{ cm}^{-3}$, $2 \times 10^{17} \text{ cm}^{-3}$, and $7.5 \times 10^{16} \text{ cm}^{-3}$). Only values in this range lead to satisfactory agreement.

The polarization versus applied voltage, extracted from the simulations, is shown in Fig. 3(a). One can clearly identify *P-V* hysteresis loops for each free carrier concentration. The upper and lower horizontal lines in each *P-V* hysteresis loop correspond to the saturation polarizations $P_{\text{sat,max}}$ and $P_{\text{sat,min}}$, which increase with carrier concentration [Fig. 3(b)]. Despite the application of rather high voltages with opposite polarities (corresponding to electric fields of almost $\pm 10^{10} \text{ V/m}$), no zero crossing (i.e., inversion of polarization) is found between $P_{\text{sat,max}}$ and $P_{\text{sat,min}}$. The resulting polarization remains always negative (i.e., pointing into the surface), but changes in magnitude.

The presence of a *P-V* hysteresis at 4.3 K raises the questions of the underlying physics. In order to unravel the origin of the hysteresis, we first recall the field-free case. Nonferroelectric effects are frozen out at 4.3 K temperature, as outlined above. Even the thermal rotation of the MA molecule dipoles is frozen at 4.3 K, considering the rotation barrier of 42–150 meV and attempt frequencies in the range of 10^{12} s^{-1} [42–45]. Therefore, without an external electric field an in-plane antiferroelectric MA dipole order is present in the bulk [Fig. 4(a)]. In addition, displacements of the MA⁺ ions relative to the Br[−] ions cause an out-of-plane lattice-induced polarization component $P_{\text{MA}^+\text{Br}^-}$ in the bulk [22,23,46]. All other lattice relaxation effects yield minor polarization components that can be neglected in the first approximation. The outermost surface layer is, however, typically significantly different than the bulk material. Density functional theory calculations predict that at the closely related MAPbI₃ surface

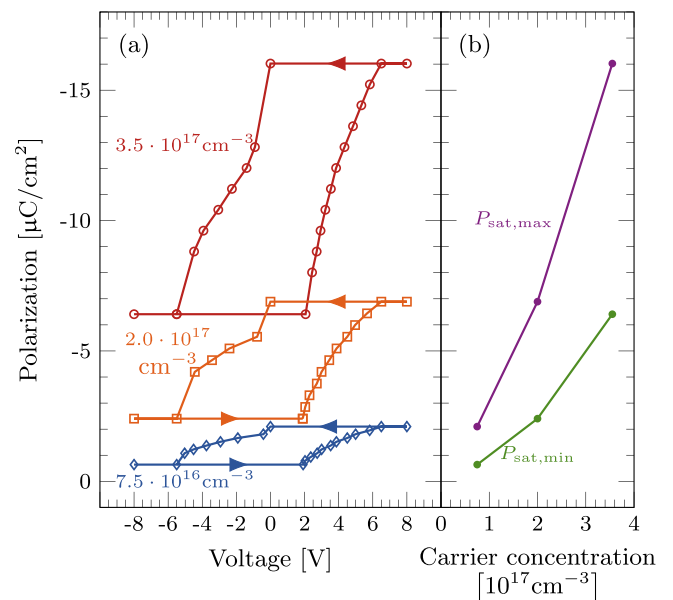


FIG. 3. (a) Extracted spontaneous polarization vs applied voltage (*P-V* hysteresis loops) for different carrier concentrations of $3.5 \times 10^{17} \text{ cm}^{-3}$ (red), $2 \times 10^{17} \text{ cm}^{-3}$ (orange), and $7.5 \times 10^{16} \text{ cm}^{-3}$ (blue). The voltage sweep direction is indicated by arrowheads. The *P-V* hysteresis loops are obtained by fitting computed tunnel currents to the measured *I-V* spectra (cf. Fig. 2 and text). The upper and lower horizontal lines in each hysteresis loop indicate the corresponding saturation polarizations $P_{\text{sat,max}}$ and $P_{\text{sat,min}}$, which increase with carrier concentrations, as shown in (b).

it is energetically favorable to compensate for the bulk polarization (due to the loss of symmetry) [46], by lattice relaxation and a $\sim 30^\circ$ out-of-plane rotation of the surface MA dipoles. This results in a compensating surface polarization of about $-4.3 \mu\text{C}/\text{cm}^2$ pointing into the surface [46]. We anticipate a similar compensating surface polarization structure at the MAPbBr₃ surface investigated here [Fig. 4(a)].

Next, we turn to the measured (surface) polarization under applied electric field: For all voltages, the experimentally deduced polarization is negative, i.e., points into the surface (Fig. 3). At positive sample voltages, the negative sides of the MA dipoles point towards the negative tip, thus increasing the negative surface charge. This situation is counterintuitive, as one expects the molecules to align oppositely within the zone, where the electric field penetrates into the sample, resulting in a classical *P-V* hysteresis curve changing from positive to negative polarization when reversing the voltage polarity. Instead, we observe a hysteresis shifted fully towards negative polarization.

This contradiction can be resolved, when recalling that scanning tunneling microscopy and spectroscopy probe the outermost surface layer, not to underlying bulk layers, due to the exponential decay of the tunnel current with tip-sample separation [49]. Therefore, states and polarization of the crystal interior cannot be measured directly, but rather contribute indirectly through their influence on the top surface layer, which can differ considerably from the underlying bulk. Indeed, a surface polarization reversed as compared to the

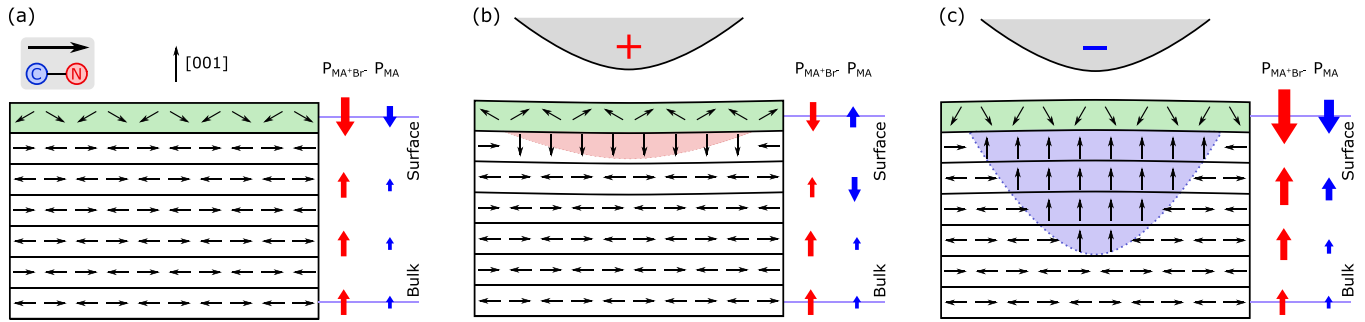


FIG. 4. Conceptual schematic showing the principle of the projected MA dipole orientation and co-occurring ion-lattice relaxation at the surface (green) layer and in subsurface/bulk (white) layers of orthorhombic MAPbBr₃. Horizontal lines correspond to single atomic layers. (a) Without external electric field an almost complete antiferroelectric MA dipole order (black arrows) is present in the bulk, with only a small polarization component pointing in the [001] direction (P_{MA} , small blue arrows). In addition, displacements of the Br⁻ ions relative to the MA⁺ ions (not shown here) cause a lattice-induced polarization component in the [001] direction ($P_{MA^+Br^-}$, red arrows). At the surface it is energetically favorable to compensate for the bulk polarization (due to the loss of symmetry) [46], by lattice relaxation and a $\sim 30^\circ$ out-of-plane rotation of the surface MA dipoles, resulting in a surface polarization pointing in the [001] direction. (b) In the presence of a positively biased tip (negative sample voltage) the electric field penetrates the MAPbBr₃ crystal, causing an alignment of the MA dipoles in the [001] direction (light red shaded area), and a concomitant lattice-related polarization $P_{MA^+Br^-}$ decrease due to an out-of-plane displacement of the MA molecules [8,44,47]. Hence, $P_{MA^+Br^-}$ and P_{MA} are oriented antiparallel, weakening the overall polarization, as compared to the field-free case. The bulk polarization is again compensated at the surface by an oppositely directed surface polarization, but smaller than in the field-free case in (a). Note, the penetration of the electric field is rather small for positive tip (negative sample) voltages, since the downward band bending induces an electron accumulation zone, which provides a highly efficient screening. However, the lateral and vertical extent of the alignment depends on the tip radius and tip-sample separation and is not to scale in the conceptual schematic. (c) In the case of a negatively biased tip (positive sample voltage) the MA dipoles in the subsurface region are field aligned in the [001] direction (light blue shaded area). As a result, $P_{MA^+Br^-}$ and P_{MA} are oriented parallel, leading to a strengthening of the overall polarization in the subsurface region and of the compensating polarization at the surface as compared to the field-free case in (a). In addition, a piezoelectric effect occurs [48] due to the field-induced distortion and tilting of the Br octahedra [44]. This deforms the lattice in the ferroelectrically ordered field penetrated zone, resulting in the observed increase of tip-sample separation.

underlying bulk has been theoretically predicted to exist at MAPbI₃ single-crystal surfaces [46].

On this basis we can elucidate the effect of the applied field: An applied electric field is known to penetrate into the semiconductor bulk, due to limited screening. The typical penetration depth is in the range of 10–100 nm. The subsurface MA molecules within this penetration depth can be field-rotated [Figs. 4(b) and 4(c)]. This is possible because the dipole-dipole interaction energy of 25 meV is smaller than the energy $W = -p \cdot E \sim 170$ meV of a dipole p in an electric field E in the order of 4×10^9 V/m [13]. With increasing voltage, the penetration depth of the electric field increases, causing molecules to align in deeper and deeper regions, increasing the dipole-induced polarization component P_{MA} . This leads to a weakening (strengthening) of the total polarization in the crystal interior at negative (positive) sample voltages. In analogy to the field-free case, we anticipate that the loss of symmetry at the surface leads, in the first approximation again, to a compensating surface polarization, which is weakened (strengthened) at negative (positive) sample voltages [Figs. 4(b) and 4(c)].

With this model, the measured hysteresis can be understood quantitatively. The polarization value in the center of the hysteresis curve in Fig. 3(a) reflects the surface polarization under field-free conditions. The expected value of about $-4.3 \mu\text{C}/\text{cm}^2$ fits best to the orange P - V hysteresis corresponding to a carrier concentration of $2 \times 10^{17} \text{ cm}^{-3}$. The magnitude of the hysteresis of about $\pm 2 \mu\text{C}/\text{cm}^2$ also fits well to the

maximal magnitude of polarization induced by full molecule dipole alignment of about $1.6 \mu\text{C}/\text{cm}^2$ [46]. This suggests that in the crystal interior the molecules are indeed aligned and at the surface the polarization change is compensated.

Thus far we discussed the out-of-plane surface polarization under the influence of an electric field. In plane, the dimer structure observed in STM images and current imaging tunneling spectroscopy (CITS) maps at all applied voltages [Fig. 1(c)] demonstrate the presence of an in-plane antiferroelectric head-to-head dipole arrangement, which is independent of the applied electric field [as indicated in the inset of Fig. 1(b)]. Hence, this in-plane dipole order appears to be pinned at the surface. Only the additional out-of-plane rotation of the dipoles is responsible for the compensating surface polarization and is modulated by applying an electric field.

Furthermore, the alignment of the molecules in the crystal interior is directly connected to a structural relaxation, since molecule orientation and octahedral tilting interact [42,43]. This relaxation induces an ion-lattice polarization component $P_{MA^+Br^-}$ in the [001] direction (cf. red arrows in Fig. 4) in addition to the molecule dipole polarization component P_{MA} . The ion-lattice relaxation leads to a change of the c -lattice constant [44] which in turn affects the tip-sample separation. In the first approximation the tip-sample separation is then proportional to the penetration depth of the electric field (i.e., the molecule alignment) and thus the polarization and tip-sample separation can be anticipated to be proportional, as

assumed above. This is in line with reported piezoelectricity [50]. The existence of the ion-lattice relaxation is corroborated by the different tip-sample separations extracted from the tunneling spectra at the voltage end points.

Finally, for the existence of a hysteresis it is critical that the field-induced rotation of the molecules is self-sustaining after turning off the electric field. This remanent polarization arises from the existence of a rotation barrier and the dipole-dipole interaction energy. Both are much larger than the thermal energy at 4.3 K. Only if sufficiently large voltages with reversed polarity are applied, a field-induced reorientation of the molecules takes place. This gives rise to a remanent polarization and hence hysteresis on the timescale of the voltage sweep.

In conclusion, we provide direct evidence of a field-induced rotation and alignment of subsurface methylammonium molecular dipoles, combined with an ion-lattice relaxation in orthorhombic MAPbBr₃ (001) at 4.3 K using scanning tunneling spectroscopy. The field-induced polarization in the bulk is compensated at the surface by an oppositely oriented, counteracting out-of-plane polarization component

of the otherwise in-plane antiferroelectrically ordered surface dipole arrangement. The results reveal the existence of a ferroelectric *P-V* hysteresis at 4.3 K, stabilized by the MA molecule dipole-dipole interaction. This suggests that at low temperatures only ferroelectric effects govern the hysteresis in MAPbBr₃ and its related compounds, whereas at high temperatures thermally activated processes such as ion migration and charge trapping-detrapping dominate and override the dipole-dipole interaction. Finally, the method used here for extracting the polarization from tunneling spectroscopy is widely applicable to many other materials beyond metalorganic halide perovskites, providing direct access to quantify surface polarization and compensation of bulk polarization at surfaces.

The authors thank the Deutsche Forschungsgemeinschaft (Grant No. 447951695), the National Science and Technology Council (NSTC) Taiwan (Grants No. NSTC 112-2119-M-002-021-MBK and No. NSTC 109-2628-M-002-005-MY3), and the National Taiwan University (Grants No. NTU-112L7711 and No. NTU-112L7813) for financial support.

-
- [1] S. Sajid, A. M. Elseman, J. Ji, S. Dou, D. Wei, H. Huang, P. Cui, W. Xi, L. Chu, Y. Li, B. Jiang, and M. Li, *Nano-Micro Lett.* **10**, 51 (2018).
- [2] S. Sahare, P. Ghoderao, S. B. Khan, Y. Chan, and S.-L. Lee, *Nanoscale* **12**, 15970 (2020).
- [3] National Renewable Energy Laboratory (NREL), Best Research-Cell Efficiency Chart, at <https://www.nrel.gov/pv/cell-efficiency.html> (2022), accessed 06/02/2022.
- [4] J. A. Christians, J. S. Manser, and P. V. Kamat, *J. Phys. Chem. Lett.* **6**, 852 (2015).
- [5] H. J. Snaith, A. Abate, J. M. Ball, G. E. Eperon, T. Leijtens, N. K. Noel, S. D. Stranks, J. T.-W. Wang, K. Wojciechowski, and W. Zhang, *J. Phys. Chem. Lett.* **5**, 1511 (2014).
- [6] A. C. Ferreira, A. Létoublon, S. Paofai, S. Raymond, C. Ecolivet, B. Rufflé, S. Cordier, C. Katan, M. I. Saidaminov, A. A. Zhumekenov, O. M. Bakr, J. Even, and P. Bourges, *Phys. Rev. Lett.* **121**, 085502 (2018).
- [7] X. Zhang and S.-H. Wei, *Phys. Rev. Lett.* **128**, 136401 (2022).
- [8] A. Stroppa, C. Quarti, F. De Angelis, and S. Picozzi, *J. Phys. Chem. Lett.* **6**, 2223 (2015).
- [9] Z. Fan, J. Xiao, K. Sun, L. Chen, Y. Hu, J. Ouyang, K. P. Ong, K. Zeng, and J. Wang, *J. Phys. Chem. Lett.* **6**, 1155 (2015).
- [10] G. A. Sewvandi, K. Kodera, H. Ma, S. Nakanishi, and Q. Feng, *Sci. Rep.* **6**, 30680 (2016).
- [11] Y. Rakita, O. Bar-Elli, E. Meirzadeh, H. Kaslasi, Y. Peleg, G. Hodes, I. Lubomirsky, D. Oron, D. Ehre, and D. Cahen, *Proc. Natl. Acad. Sci. USA* **114**, E5504 (2017).
- [12] Z.-R. Gao, X.-F. Sun, Y.-Y. Wu, Y.-Z. Wu, H.-L. Cai, and X. S. Wu, *J. Phys. Chem. Lett.* **10**, 2522 (2019).
- [13] J. M. Frost, K. T. Butler, F. Brivio, C. H. Hendon, M. van Schilfgaarde, and A. Walsh, *Nano Lett.* **14**, 2584 (2014).
- [14] Z. Xiao, Y. Yuan, Y. Shao, Q. Wang, Q. Dong, C. Bi, P. Sharma, A. Gruverman, and J. Huang, *Nat. Mater.* **14**, 193 (2015).
- [15] S. Meloni, T. Moehl, W. Tress, M. Franckevičius, M. Saliba, Y. H. Lee, P. Gao, M. K. Nazeeruddin, S. M. Zakeeruddin, U. Rothlisberger, and M. Graetzel, *Nat. Commun.* **7**, 10334 (2016).
- [16] M. Stumpp, R. Ruess, J. Horn, J. Tinz, C. Richter, and D. Schlottwein, *Phys. Status Solidi A* **213**, 38 (2016).
- [17] C.-J. Tong, W. Geng, O. V. Prezhdo, and L.-M. Liu, *ACS Energy Lett.* **2**, 1997 (2017).
- [18] L. McGovern, M. H. Futscher, L. A. Muscarella, and B. Ehrler, *J. Phys. Chem. Lett.* **11**, 7127 (2020).
- [19] A. Musiienko, J. Pipek, P. Praus, M. Brynza, E. Belas, B. Dryzhakov, M.-H. Du, M. Ahmadi, and R. Grill, *Sci. Adv.* **6**, eabb6393 (2020).
- [20] X. Huang, T. R. Paudel, P. A. Dowben, S. Dong, and E. Y. Tsymbal, *Phys. Rev. B* **94**, 195309 (2016).
- [21] Within the dominating dimer structure, thin zigzag structure insertions, typically 1 nm wide, occur [51]. The two structures differ in their in-plane, but not in their out-of-plane MA molecule orientation. Hence, the following analysis is not affected by the thin insertions. Note, on both sides of the ~ 1 -nm-wide zigzag insertion the change of in-plane molecule orientation induces sheet charges of opposite sign. Their separation is well below the screening length and hence cannot be detected in STM.
- [22] R. Ohmann, L. K. Ono, H.-S. Kim, H. Lin, M. V. Lee, Y. Li, N.-G. Park, and Y. Qi, *J. Am. Chem. Soc.* **137**, 16049 (2015).
- [23] L. She, M. Liu, and D. Zhong, *ACS Nano* **10**, 1126 (2016).
- [24] X. Che, B. Traore, C. Katan, M. Kepenekian, and J. Even, *Phys. Chem. Chem. Phys.* **20**, 9638 (2018).
- [25] H.-C. Hsu, B.-C. Huang, S.-C. Chin, C.-R. Hsing, D.-L. Nguyen, M. Schnedler, R. Sankar, R. E. Dunin-Borkowski, C.-M. Wei, C.-W. Chen, Ph. Ebert, and Y.-P. Chiu, *ACS Nano* **13**, 4402 (2019).
- [26] R. M. Feenstra and J. A. Stroschio, *J. Vac. Sci. Technol. B* **5**, 923 (1987).
- [27] R. M. Feenstra, Y. Dong, M. P. Semtsiv, and W. T. Masselink, *Nanotechnol.* **18**, 044015 (2007).
- [28] G. Binnig, K. H. Frank, H. Fuchs, N. Garcia, B. Reihl, H. Rohrer, F. Salvan, and A. R. Williams, *Phys. Rev. Lett.* **55**, 991 (1985).

- [29] The mobility of free charge carriers in MAPbBr₃ single crystals is in the order of 100 cm²/Vs [52]. For an applied electric field in the order of 4×10^9 V/m, the drift velocity is thus approximately 4×10^7 m/s. Hence, the free carriers in a typical tip-induced band bending region with a depth of 100 nm can redistribute in less than 2.5 fs to compensate a change in the electric field.
- [30] Ion migration and drift (of Br⁻, V_{Br}⁺, MA⁺, Pb²⁺, and as impurity H⁺) can be excluded at 4.3 K, considering diffusion coefficients of 10^{-15} – 10^{-8} cm²/s [53–59] at room temperature and activation energies of 1.41 down to 0.25 eV [18,58,60]. Charge trapping-detrapping [19] can be excluded, since carriers in deep traps cannot be thermally excited at 4.3 K and the electric field is too small for a field-induced detrapping.
- [31] S. Govinda, B. P. Kore, M. Bokdam, P. Mahale, A. Kumar, S. Pal, B. Bhattacharyya, J. Lahnsteiner, G. Kresse, C. Franchini, A. Pandey, and D. D. Sarma, *J. Phys. Chem. Lett.* **8**, 4113 (2017).
- [32] M. Schnedler, V. Portz, P. H. Weidlich, R. E. Dunin-Borkowski, and Ph. Ebert, *Phys. Rev. B* **91**, 235305 (2015).
- [33] M. Schnedler, R. E. Dunin-Borkowski, and Ph. Ebert, *Phys. Rev. B* **93**, 195444 (2016).
- [34] Y. Wang, M. Schnedler, Q. Lan, F. Zheng, L. Freter, Y. Lu, U. Breuer, H. Eisele, J.-F. Carlin, R. Butté, N. Grandjean, R. E. Dunin-Borkowski, and Ph. Ebert, *Phys. Rev. B* **102**, 245304 (2020).
- [35] N. Onoda-Yamamuro, T. Matsuo, and H. Suga, *J. Phys. Chem. Solids* **53**, 935 (1992).
- [36] P. Schulz, E. Edri, S. Kirmayer, G. Hodes, D. Cahen, and A. Kahn, *Energy Environ. Sci.* **7**, 1377 (2014).
- [37] G. Papavassiliou and I. Koutselas, *Synth. Met.* **71**, 1713 (1995).
- [38] N. Kitazawa, Y. Watanabe, and Y. Nakamura, *J. Mater. Sci.* **37**, 3585 (2002).
- [39] J. H. Noh, S. H. Im, J. H. Heo, T. N. Mandal, and S. I. Seok, *Nano Lett.* **13**, 1764 (2013).
- [40] F. Chen, C. Zhu, C. Xu, P. Fan, F. Qin, A. Gowri Manohari, J. Lu, Z. Shi, Q. Xu, and A. Pan, *J. Mater. Chem. C* **5**, 7739 (2017).
- [41] We model the polarization termination as surface sheet charge and do not account for spatial changes of polarization with increasing subsurface depth. This provides the correct sign of field-induced polarization but due to the surface compensation effect predicted by density function theory [46], the magnitude may have a slight systematic deviation.
- [42] J.-H. Lee, N. C. Bristowe, P. D. Bristowe, and A. K. Cheetham, *Chem. Commun.* **51**, 6434 (2015).
- [43] O. Selig, A. Sadhanala, C. Müller, R. Lovrincic, Z. Chen, Y. L. A. Rezus, J. M. Frost, T. L. C. Jansen, and A. A. Bakulin, *J. Am. Chem. Soc.* **139**, 4068 (2017).
- [44] D. Ji, M. Na, S. Wang, H. Zhang, K. Zhu, C. Zhang, and X. Li, *Sci. Rep.* **8**, 12492 (2018).
- [45] T. Debnath, D. Sarker, H. Huang, Z.-K. Han, A. Dey, L. Polavarapu, S. V. Levchenko, and J. Feldmann, *Nat. Commun.* **12**, 2629 (2021).
- [46] T.-Y. Zhu and D.-J. Shu, *J. Phys. Chem. Lett.* **12**, 3898 (2021).
- [47] L. Leppert, S. E. Reyes-Lillo, and J. B. Neaton, *J. Phys. Chem. Lett.* **7**, 3683 (2016).
- [48] H. Park, C. Ha, and J.-H. Lee, *J. Mater. Chem. A* **8**, 24353 (2020).
- [49] M. Schnedler, Y. Jiang, K.H.Wu, E. Wang, R. Dunin-Borkowski, and Ph. Ebert, *Surf. Sci.* **630**, 225 (2014).
- [50] M. Coll, A. Gomez, E. Mas-Marza, O. Almora, G. Garcia-Belmonte, M. Campoy-Quiles, and J. Bisquert, *J. Phys. Chem. Lett.* **6**, 1408 (2015).
- [51] B.-C. Huang, P. Yu, Y. H. Chu, C.-S. Chang, R. Ramesh, R. E. Dunin-Borkowski, P. Ebert, and Y.-P. Chiu, *ACS Nano* **12**, 1089 (2018).
- [52] Y. Cho, H. R. Jung, Y. S. Kim, Y. Kim, J. Park, S. Yoon, Y. Lee, M. Cheon, S.-y. Jeong, and W. Jo, *Nanoscale* **13**, 8275 (2021).
- [53] A. Senocrate, I. Moudrakovski, G. Y. Kim, T.-Y. Yang, G. Gregori, M. Grätzel, and J. Maier, *Angew. Chem., Int. Ed.* **56**, 7755 (2017).
- [54] L. Bertoluzzi, R. A. Belisle, K. A. Bush, R. Cheacharoen, M. D. McGehee, and B. C. O'Regan, *J. Am. Chem. Soc.* **140**, 12775 (2018).
- [55] C. Li, A. Guerrero, S. Huettner, and J. Bisquert, *Nat. Commun.* **9**, 5113 (2018).
- [56] A. Senocrate, I. Moudrakovski, T. Acartürk, R. Merkle, G. Y. Kim, U. Starke, M. Grätzel, and J. Maier, *J. Phys. Chem. C* **122**, 21803 (2018).
- [57] W. Peng, C. Aranda, O. M. Bakr, G. Garcia-Belmonte, J. Bisquert, and A. Guerrero, *ACS Energy Lett.* **3**, 1477 (2018).
- [58] M. H. Futscher, J. M. Lee, L. McGovern, L. A. Muscarella, T. Wang, M. I. Haider, A. Fakharuddin, L. Schmidt-Mende, and B. Ehrler, *Mater. Horiz.* **6**, 1497 (2019).
- [59] M. García-Battle, J. Mayén Guillén, M. Chapran, O. Baussens, J. Zaccaro, J.-M. Verilhac, E. Gros-Daillon, A. Guerrero, O. Almora, and G. Garcia-Belmonte, *ACS Energy Lett.* **7**, 946 (2022).
- [60] C. Lin, S. Li, W. Zhang, C. Shao, and Z. Yang, *ACS Appl. Energy Mater.* **1**, 1374 (2018).